Journal of Thermal Analysis and Calorimetry (2020) 139:2577–2583
https://doi.org/10.1007/s10973-019-08583-0

Second-law thermodynamic analysis on non-premixed counterflow methane flames with hydrogen addition

Yusen Liu[1] · Jiabo Zhang[1] · Dehao Ju[1] · Liuliu Shi[2] · Dong Han[1]

Received: 30 May 2019 / Accepted: 14 July 2019 / Published online: 26 July 2019

Abstract

Natural gas is an attractive alternative fuel because of its environment-friendly nature, and hydrogen addition is considered as an efficient method to improve the methane combustion performance in combustion engines. In this study, the exergy destruction characteristics in non-premixed counterflow methane flames are numerically studied based on the second law of thermodynamics. The irreversible processes during combustion, such as heat conduction, mass diffusion and chemical reactions, are studied, and it is found that heat conduction is the dominant factor in exergy destruction. Additionally, the exergy destruction from each source shows two peaks, and their overall impact causes the total exergy destruction to exhibit three peaks. Moreover, the effects of hydrogen addition on exergy destruction from each source are evaluated. The effect of hydrogen addition on the exergy destruction from heat conduction is insignificant, and the exergy destruction from mass diffusion increases with hydrogen addition. For the exergy destruction from chemical reactions, the carbon-containing reactions are key to the first peak of the exergy destruction rate, whereas the H_2-O_2 system reactions are more important for the second peak. The contribution of chemical reactions to the overall exergy destruction decreases with H_2 addition.

Keywords Second law of thermodynamics · Non-premixed flame · Counterflow · Methane · Hydrogen

Introduction

Natural gas (NG) has a higher hydrogen-to-carbon ratio than the other hydrocarbon fuels. Therefore, NG usage in transportation sectors may be beneficial for the reduction of carbon dioxide and particulate matter emissions, and it is as such considered as an alternative transportation fuel. However, NG engines encounter problems in application, such as lower engine efficiency [1] and higher combustion instability [2] due to its low flame speed. The addition of H_2, a fuel with fast flame propagation, was considered as a method to solve these problems [3]. Therefore, combustion and emissions characteristics of engines fueled with NG and H_2 blends have been widely studied [4–7]. Gong et al. [8] pointed that with H_2 addition, the ignition delay in natural gas engines was shortened and the engine-out emissions were reduced, but Verma and Prasad [9] found that the knock tendency of a compressed natural gas engine increased with H_2 addition at high loads.

Thermal efficiency is an important parameter for engine performance evaluation and is conventionally calculated based on the first law of thermodynamics. However, the first law of thermodynamics is limited to energy quantity analysis, without considering the energy quality change in energy conversion processes. Recently, the second-law thermodynamic analysis has been applied by some researchers to study the energy conversion in thermodynamic systems [10, 11], from which the energy quality changes could be evaluated. By applying the second law of thermodynamics to engine efficiency analysis, Rakopoulos and Michos [12] concluded that the combustion irreversibility is a primary source for exergy destruction. Therefore, it is significant to understand the energy quality

✉ Dong Han
dong_han@sjtu.edu.cn

[1] Key Laboratory for Power Machinery and Engineering, Ministry of Education, Shanghai Jiao Tong University, Shanghai 200240, China

[2] School of Energy and Power Engineering, University of Shanghai for Science and Technology, Shanghai 200093, China

degradation mechanism in combustion processes, based on which methods for efficiency improvement might be explored. Recently, Zhang et al. [13, 14] attempted to elucidate the exergy destruction sources in fuel auto-ignition and flame propagation [15, 16], based on an analysis combining thermochemistry and chemical kinetics. It was found that exergy destruction in fuel combustion might be reduced by proper fuel blending or charge preparation.

There are two types of NG engines based on the mixture preparation methods, i.e., the premixed charge spark-ignited NG engines and diesel/NG dual-fuel engines, the latter of which features the mixing-controlled combustion. These distinct combustion organization methods require researchers to identify exergy destruction characteristics in both premixed and non-premixed CH_4 flames. Wang et al. [17] investigated the entropy generation in premixed methane/hydrogen flames using a multi-step kinetic model, and they found that with H_2 addition, the total exergy destruction decreased because of the reduced entropy generation from thermal conduction. Besides, Emadi and Emami [18] studied the effects of H_2 addition on the irreversibility in turbulent non-premixed methane flames, and they indicated that H_2 enrichment increased the second-law combustion efficiency and reduced the total entropy generation. Chen et al. [19] investigated the influence of the effective equivalence ratio and H_2 enrichment in fuel mixtures on the entropy generation in lean methane/air counterflow non-premixed flames and found that the total entropy generation increased with H_2 fraction and effective equivalence ratio.

Although there already were some studies aiming to figure out the exergy destruction characteristics in different non-premixed CH_4/H_2 flames, they were mainly focused on parametric studies and the physical/chemical mechanisms underlying exergy destruction in non-premixed flames have not been well identified. In this study, the thermochemical and chemical kinetic analysis was combined to explain the exergy destruction mechanism in non-premixed counterflow flames of methane and hydrogen mixtures. The contributions of different sources to exergy destruction in the context of changed H_2 percentage were studied, with the influence of each parameter on exergy destruction being elucidated.

Methodology

The one-dimensional counterflow non-premixed flames were simulated at atmospheric pressure using the GRI 3.0 Mech [20] and the CHEMKIN PRO software [21]. This mechanism has been widely validated against the experimental measurements, such as flame propagation [22], soot formation [23] and auto-ignition tendency [24]. Further, Cheng et al. [25] and Padilla et al. [26] compared the experimentally measured mole fractions of primary species, peak temperature and temperature profiles in methane counterflow flames with the calculated results using the GRI 3.0 Mech, and the comparison showed that the experimental and computational results are in good agreement. As such, GRI 3.0 Mech was used for the calculation in this study. For all the studied conditions, the unburned gas temperature and the environmental temperatures were held at 300 K and 298 K, respectively. Equal flow velocities at the fuel and oxidizer nozzle exits were set, and the distance between the two nozzles was set as 3 cm. The thermodynamic and chemical data used for exergy destruction calculation, e.g., temperature, pressure, mole fractions of species and reaction rates, could be obtained in the calculation results.

Exergy destruction is caused by entropy generation, and the entropy generation in flames includes four irreversible sources, namely heat conduction, mass diffusion, viscous dissipation and chemical reactions. Therefore, the total entropy generation is calculated by Eq. 1 [27]:

$$\dot{S}_g = -\frac{\dot{q}_c \cdot \nabla T}{T^2} - \frac{1}{T}\sum_i [\dot{m}_i \cdot (s_i \nabla T + \nabla \mu_i)] + \frac{\tau : \nabla u}{T} + \sum_i \frac{f_i \cdot \dot{m}_i}{T} - \frac{\mu_i \cdot \dot{\omega}_i}{T} \quad (1)$$

where T is the temperature, $\dot{q}_c$ is the flux of heat conduction, $\dot{m}_i$ is the mass flux of the ith species, s_i is the specific entropy of the ith species, τ is the friction stress, u is the velocity, f_i is the body force of the ith species, μ_i is the chemical potential of the ith species and $\dot{\omega}_i$ is the molar production rate of the ith species. The terms on the right side of Eq. 1 represent the entropy generation rates induced by heat conduction, mass diffusion, viscous dissipation, body force and chemical reactions, respectively.

According to the Fourier's law,

$$q_c = -\lambda \nabla T \quad (2)$$

where λ is the thermal conductivity.

According to the Fick's law,

$$\dot{m}_i = -\rho D_i \nabla Y_i \quad (3)$$

where ρ is the mass density of the gas, D_i is the diffusion coefficient of the ith species and Y_i is the mole fraction of the ith species.

The gravity is the only body force considered here, and thus,

$$\sum_i f_i \cdot \dot{m}_i = \sum_i g \cdot \dot{m}_i = g \cdot \sum_i \dot{m}_i = 0 \quad (4)$$

Therefore, the one-dimensional form of Eq. 1 could be expressed as Eq. 5:

$$S_g = \frac{\lambda \nabla T \cdot \nabla T}{T^2} + R \sum_i \frac{\rho D_i}{X_i} \nabla Y_i \cdot \nabla X_i + \frac{\tau : \nabla u}{T} - \frac{\mu_i \cdot \dot{\omega}_i}{T} \quad (5)$$

where R is the gas constant and X_i is the mole fraction of the ith species.

According to Nishida et al. [28], the entropy generation from viscous dissipation is negligible compared with those from the other sources. Therefore, the entropy generation due to viscous dissipation is not considered in the following study.

After calculating the entropy generation, the exergy destruction rate can be presented as Eq. 6 [29]:

$$\dot{I}_{destruction} = T_0 \dot{S}_g \quad (6)$$

where T_0 is the environment temperature, i.e., 298 K.

Therefore, the exergy destruction rates from heat conduction, mass diffusion and chemical reactions can be calculated as follows:

$$\dot{I}_{cond} = T_0 \lambda \frac{1}{T^2} \left(\frac{dT}{dx} \right)^2 \quad (7)$$

$$\dot{I}_{diff} = T_0 \sum_{k=1}^{k} \frac{\rho R_{gi} D_i}{X_i} \frac{dY_i}{dx} \frac{dX_i}{dx} \quad (8)$$

$$\dot{I}_{chem} = -T_0 \sum_i \frac{\mu_{i,j} \dot{\omega}_{i,j}}{T} \quad (9)$$

where R_{gi} is the specific gas constant of the ith species, $\mu_{i,j}$ and $\dot{\omega}_{i,j}$ are the chemical potential and the mole production rate of the ith species in the jth reaction.

The chemical potential in Eq. 9 can be expressed as:

$$\mu_{i,j} = -T s_{i,j}(T_i) + h_{i,j}(T_i) + RT \ln(X_i P_i) \quad (10)$$

where $s_{i,j}(T_i)$ and $h_{i,j}(T_i)$ are the specific entropy and enthalpy of the ith species in the jth reaction, respectively, and T_i and P_i are the temperature and partial pressure of the ith species.

Fuel chemical exergy injected from nozzles changes with changed H_2 blending percentage. Therefore, it is not appropriate to directly compare the absolute exergy destruction amount in different fuels. To clearly compare the exergy destruction behaviors in different CH_4/H_2 flames, normalized exergy destruction was used in this study. Specifically, the fuel chemical exergy can be calculated by Eq. 11:

$$E_{burned} = (1 - \varphi_{un}) \cdot \rho_{fuel} \cdot u_{in} \cdot e_{fuel} \quad (11)$$

where φ_{un} is in the fraction of unburned fuel, ρ_{fuel} is the fuel density, u_{in} is the fuel flow velocity, and e_{fuel} is the specific chemical exergy. The normalized exergy destruction can be calculated as Eq. 12:

$$\bar{I}_{destruction} = \frac{\dot{I}_{destruction}}{E_{burned}} \quad (12)$$

where $\bar{I}_{destruction}$ is the normalized exergy destruction rates.

As described above, exergy destruction characteristics in non-premixed counterflow flames of CH_4/H_2 blends and air were analyzed based on thermodynamics and chemical kinetics. Specifically, the exergy destruction in flames of 100%CH_4 and 50%CH_4–50%H_2 was compared.

Results and discussion

To explain the exergy destruction in non-premixed counterflow flames, the CH_4/air flame is first taken as the baseline case, in which the flow velocities at both nozzle exits are set as 15 cm/s. As shown in Fig. 1, the total normalized exergy destruction rate curve has three peaks, the first and the third of which are caused by heat conduction, while the second is mainly induced by chemical reactions. In addition, all the normalized exergy destruction rate profiles of heat conduction, mass diffusion and chemical reactions feature double peaks. It is shown that the highest peak is caused by chemical reactions and located at the flame center, followed by the peaks from heat conduction and mass diffusion. It is also observed that the second peak of the normalized exergy destruction rate from chemical reactions is located at the flame downstream and much lower than the first peak, due to the much lower reaction rates at the flame downstream. Additionally, the two peaks of normalized exergy destruction rates from heat conduction occur at the flame edges, where the temperatures are low but temperature gradients are high, and this as such leads to high exergy destruction rates by heat conduction, according to Eq. 7. Finally, for the normalized exergy destruction rates from mass diffusion, the first peak

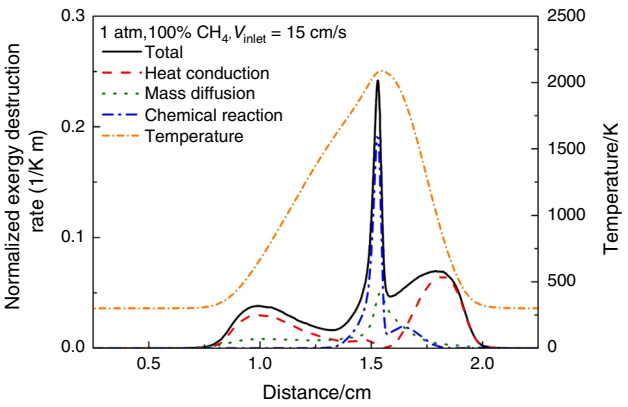

Fig. 1 Normalized exergy destruction rates and temperature profile in the non-premixed CH_4/air counterflow flame: P = 1 atm, V_{inlet} = 15 cm/s

is insignificant, and the location of the second peak is close to the flame front, where the mole fractions of species change greatly, thus causing high peak exergy destruction rate from mass diffusion, according to Eq. 8.

The contributions to exergy destruction from different sources in the flames of CH_4 and the 50%CH_4–50%H_2 blendare shown in Fig. 2. It is observed that heat conduction contributes the most to the exergy destruction in both flames, followed by chemical reactions and mass diffusion in the CH_4 flame, and by mass diffusion and chemical reactions in the flame of the 50%CH_4–50%H_2 blend. With H_2 addition, the contribution of heat conduction and mass diffusion is promoted by 1.81% and 0.92%, while that of chemical reactions is reduced by 1.72%, causing the total exergy destruction to increase by about 1%.

To explain this phenomenon, the normalized exergy destruction rates in the flames of CH_4 and the 50%CH_4–50%H_2 blend are compared in Fig. 3. It is shown that with H_2 addition, the flame region is widened and the peak temperature is raised because H_2 is more active and has higher diffusivity. The double peaks of the normalized exergy destruction rates from heat conduction are almost unaffected, possibly because the temperature profiles and temperature gradients are not significantly changed at flame edges. Therefore, the promoted contribution from heat conduction is mainly caused by the widened flame region.

Additionally, the first peak of the normalized exergy destruction rate from mass diffusion does not change much, but the second peak is slightly reduced with H_2 addition. However, considering the widened flame region, the overall contribution of mass diffusion to exergy destruction is promoted. Based on Eq. 8, the exergy destruction rate from mass diffusion is dominated by the mole fraction gradient of species. To clearly identify the exergy destruction from mass diffusion, the mole fractions of primary species, e.g., CH_4, H_2, O_2, N_2, H, O, H_2O and CO_2, are plotted in Fig. 4. Also, the contributions of these species to the two peaks of the exergy destruction from mass diffusion are listed in Tab. 1. For the flame of 100%CH_4, it is shown that CH_4 and N_2 are the dominant species in the first peak of exergy destruction by mass diffusion, as their mole fraction gradients are higher than the other species. However, in the second peak, the species H_2, H and O_2 are more influential. When considering the whole flame domain, H_2, O_2, H_2O, CH_4 and N_2 contribute most to the exergy destruction from mass diffusion, as they are the main reactants/products or the main air component. With H_2 addition, the contributions of H_2, H and H_2O to exergy destruction from mass diffusion are promoted, whereas those of the carbon-containing species are reduced. According to Fig. 4, in the first peak, the mole fraction gradients of CH_4 and N_2 in the flame of CH_4 are nearly equal to those of CH_4, H_2 and N_2 in the flame of the blend, and thus, the first peak of exergy destruction rate in both flames is almost the same. In the second peak, with H_2 addition, the change of species mole fraction exists in a wider region, and therefore, the peak mole fraction decreases, leading to the reduced peak normalized exergy destruction rates (Table 1).

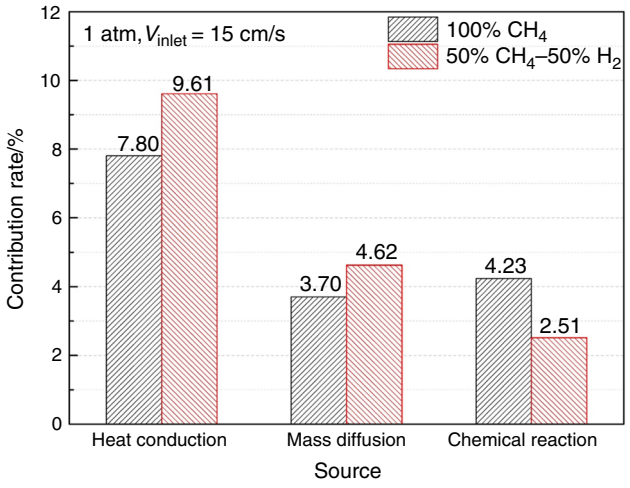

Fig. 2 Contributions to exergy destruction from each source in the flames of CH_4 and a CH_4/H_2 blend: P = 1 atm, V_{inlet} = 15 cm/s

As shown in Fig. 3, for the normalized exergy destruction rates from chemical reactions, the first peak is reduced to one-fifth and the second peak is reduced to about two-thirds with H_2 addition, causing reduced contribution of chemical reactions to exergy destruction. To further study this phenomenon, the contributions of top reactions to the two exergy destruction peaks of both fuels are listed in Tab. 2. These reactions contribute over 60% to the exergy destruction from chemical reactions, and therefore, the analysis of these reactions can help understand the exergy destruction from chemical reactions. It is obvious that in the first peak, the reactions involving carbon-containing species are more influential, while the second peak is dominated by the H_2-O_2 system reactions (Table 2).

As shown in Fig. 4, H_2 addition leads to the decreased mole fraction of CH_4, and as such, most carbon-containing reactions are suppressed. This reduces the first peak of the exergy destruction rate from chemical reactions. In addition, H_2 addition results in an increased mole fraction of H_2 and H_2O, and as such, the reactions such as R1, R6 and R9, in which H_2 and H_2O are products, are suppressed. Therefore, the first peak of the normalized exergy destruction rate from chemical reactions is reduced. In the second peak of chemical reactions, H_2 addition causes the increased mole fractions of H and H_2 and also promotes the production of H_2O. Some reactions are enhanced with H_2 addition, such as R16, R17, R21 and R24, but the others

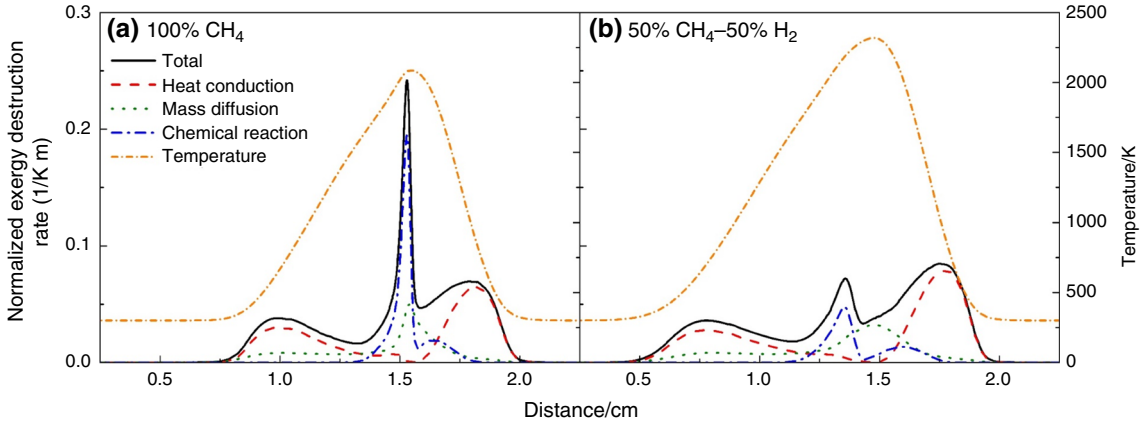

Fig. 3 Normalized exergy destruction rates from each source in the flames of CH_4 and a CH_4/H_2 blend, V_{inlet} = 15 cm/s

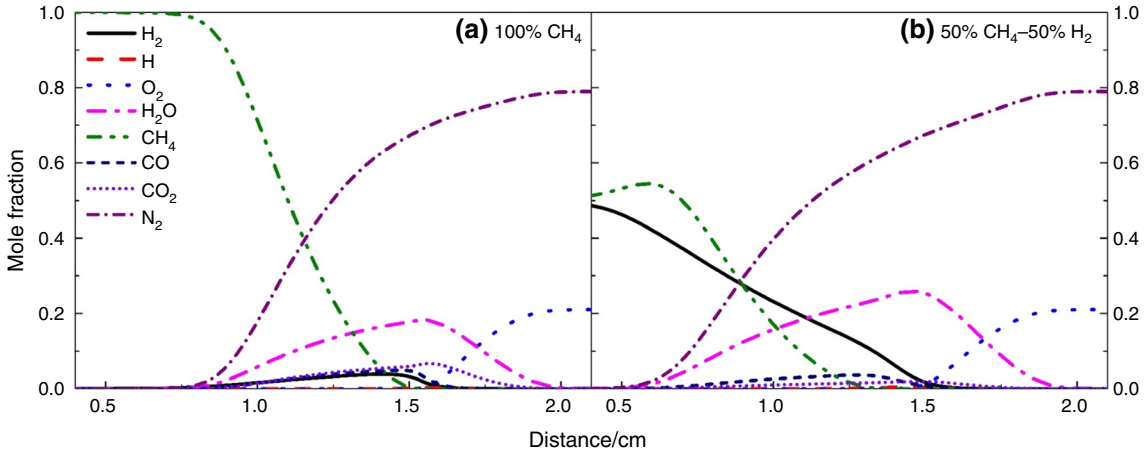

Fig. 4 Mole fraction distributions of primary species in the flames of CH_4 and a CH_4/H_2 blend, V_{inlet} = 15 cm/s

Table 1 Contributions of primary species to the exergy destruction from mass diffusion in the flames of CH_4 and a CH_4/H_2 blend, V_{inlet} = 15 cm/s

Fuel	100%CH_4			50%CH_4–50%H_2		
Species	Peak 1/%	Peak 2/%	Total/%	Peak 1/%	Peak 2/%	Total/%
H_2	0.05	0.43	0.49	0.33	1.63	1.96
H	0.00	0.18	0.19	0.00	0.27	0.27
O_2	0.00	0.42	0.44	0.00	0.53	0.53
H_2O	0.10	0.19	0.28	0.11	0.39	0.50
CH_4	0.39	0.54	0.90	0.29	0.38	0.66
CO	0.02	0.14	0.16	0.01	0.10	0.12
CO_2	0.02	0.06	0.08	0.01	0.02	0.03
N_2	0.37	0.03	0.35	0.30	0.03	0.34
Total	0.96	1.99	2.90	1.06	3.35	4.40

Table 2 Contributions of primary reactions to the exergy destruction from chemical reactions in flames of CH_4 and the 50%CH_4–50%H_2 blend, V_{inlet} = 15 cm/s

	Peak 1				Peak 2		
	Reactions	CH_4/%	CH_4–H_2 blend/%		Reactions	CH_4/%	CH_4-H_2 blend/%
R1	$H + CH_2O = HCO + H_2$	0.32	0.23	R15	$OH + HO_2 = O_2 + H_2O$	0.30	0.29
R2	$H + C_2H_4(+M) = C_2H_5(+M)$	0.22	0.14	R16	$H + O_2 + H_2O = HO_2 + H_2O$	0.17	0.18
R3	$CH + H_2O = H + CH_2O$	0.21	0.15	R17	$H + OH + M = H_2O + M$	0.07	0.10
R4	$HCO + H_2O = H+CO + H_2O$	0.18	0.10	R18	$H + O_2 + N_2 = HO_2 + N_2$	0.06	0.04
R5	$CH_2(S) + CO_2 = CO + CH_2O$	0.16	0.03	R19	$H+ HO_2 = 2OH$	0.06	0.03
R6	$OH + CH_2O = HCO + H_2O$	0.13	0.04	R20	$O + HO_2 = OH + O_2$	0.04	0.03
R7	$O + C_2H_2 = H + HCCO$	0.12	0.06	R21	$2OH(+M) = H_2O_2(+M)$	0.03	0.06
R8	$O + C_2H_2 = CO + CH_2$	0.12	0.05	R22	$H + HO_2 = O_2 + H_2$	0.03	0.01
R9	$O + CH_3 = H+H_2 + CO$	0.12	0.04	R23	$OH + H_2O_2 = HO_2 + H_2O$	0.03	0.03
R10	$HCO + M = H + CO + M$	0.12	0.05	R24	$H + O_2 = O + OH$	0.01	0.02
R11	$H + CH_2O(+M) = CH_2OH(+M)$	0.11	0.13				
R12	$H + C_2H_2(+M) = C_2H_3(+M)$	0.12	0.05				
R13	$2CH_3 = H+C_2H_5$	0.10	0.04				
	Total	2.03	1.11		Total	0.80	0.79

are suppressed, such as R15, R18, R19, R20 and R22. As a result, the overall magnitude of the second peak of the exergy destruction rate from chemical reactions is negligibly changed.

Conclusions

The second-law thermodynamic analysis on non-premixed counterflow flames of CH_4/H_2 mixtures was numerically conducted. The test fuels were 100%CH_4 and 50%CH_4–50%H_2, respectively. The sources causing exergy destruction in the flames included heat conduction, mass diffusion and chemical reactions. The main conclusions are listed as follows:

1. The total normalized exergy destruction rates feature three peaks, the first and the third of which are mainly caused by heat conduction and the second of which is dominated by chemical reactions. The normalized exergy destruction rates from heat conduction, mass diffusion and chemical reactions at most conditions show two peaks.
2. With hydrogen addition, the peaks of the normalized exergy destruction rate from heat conduction do not change much. For the exergy destruction peaks by mass diffusion, the first peak is almost unchanged because it is dominant by the unburned mixture. However, the second peak from mass diffusion is reduced, as the peak of the species mole fraction gradient decreases. The first peak of normalized exergy destruction rate from chemical reactions is reduced because the main reactions of carbon-containing species are suppressed, but the second peak is only slightly changed.
3. Heat conduction contributes the most to exergy destruction in non-premixed flames. With an increased hydrogen addition, the contributions of heat conduction and mass diffusion to exergy destruction increase, whereas the contribution of chemical reactions decreases. As a result, the total exergy destruction increases by about 1%.

Acknowledgements This research work is supported by the National Natural Science Foundation of China (Grant No. 51776124).

References

1. Chala GT, Abd Aziz A, Hagos FY. Natural gas engine technologies: challenges and energy sustainability issue. Energies Policy. 2018;11(11):2934.
2. Sofianopoulos A, Assanis DN, Mamalis S. Effects of hydrogen addition on automotive lean-burn natural gas engines: critical review. J Energy Eng. 2016;142(2):E4015010.
3. Hayder AA, Ahmad KA. HCNG fueled spark-ignition (SI) engine with its effects on performance and emissions. Renew Sustain Energy Rev. 2018;82(1):324–42.
4. Li HL, Gatts T, Liu SY, Scott Wayne, Clark N, Mather D. An experimental investigation on the combustion process of a simulated turbocharged spark ignition natural gas engine operated on stoichiometric mixture. J Eng Gas Turbines Power. 2018;140(9):091504.

5. Dumitrescu CE, Padmanaban V, Liu JD. An experimental investigation of early flame development in an optical spark ignition engine fueled with natural gas. J Eng Gas Turbines Power. 2018;140(8):082802.
6. Pan JY, Hu Z, Wei HQ, Pan MZ, Zhou L. Understanding strong knocking mechanism through high-strength optical rapid compression machines. Combust Flame. 2019;202:1–15.
7. Pan JY, Dong S, Wei HQ, Li T, Shu G, Zhou L. Temperature gradient induced detonation development inside and outside a hotspot for different fuels. Combust Flame. 2019;205:269–77.
8. Gong CM, Li ZH, Chen YL, Liu JJ, Liu FH, Han YQ. Influence of ignition timing on combustion and emissions of a spark-ignition methanol engine with added hydrogen under lean-burn conditions. Fuel. 2019;235:227–38.
9. Verma G, Prasad RK, Agarwal RA, Jain S, Agarwal AK. Experimental investigations of combustion, performance and emission characteristics of a hydrogen enriched natural gas fuelled prototype spark ignition engine. Fuel. 2016;178:209–17.
10. Gharehghani A, Hosseini R, Mirsalim M. A comparative study on the first and second law analysis and performance characteristics of a spark ignition engine using either natural gas or gasoline. Fuel. 2015;158:488–93.
11. Zhang JB, Huang Z, Han D. Effects of mechanism reduction on the energy losses analysis in n-heptane auto-ignition processes. Int J Engine Res. 2019. https://doi.org/10.1177/1468087419836870.
12. Rakopoulos CD, Michos CN. Generation of combustion irreversibilities in a spark ignition engine under biogas–hydrogen mixtures fueling. Int J Hydrogen Energy. 2009;34(10):4422–37.
13. Zhang JB, Huang Z, Han D. Exergy losses in auto-ignition processes of DME and alcohol blends. Fuel. 2018;229:116–25.
14. Zhang JB, Zhong AH, Huang Z, Han D. Second-law thermodynamic analysis in premixed flames of ammonia and hydrogen binary fuels. J Eng Gas Turbines Power. 2019;141(7):071007.
15. Zhang JB, Han D, Huang Z. Second-law thermodynamic analysis for premixed hydrogen flames with diluents of argon/nitrogen/carbon dioxide. Int J Hydrogen Energy. 2019;44(10):5020–9.
16. Zhang JB, Huang Z, Min KD, Han D. Dilution, thermal and chemical effects of carbon dioxide on the exergy destruction in n-heptane and iso-octane autoignition processes: a numerical study. Energy Fuels. 2018;32(4):5559–70.
17. Wang W, Zuo ZX, Liu JX. Entropy generation analysis of fuel premixed CH4/H-2/air flames using multistep kinetics. Int J Hydrogen Energy. 2016;41(45):20744–52.
18. Emadi A, Emami MD. Analysis of entropy generation in a hydrogen-enriched turbulent non-premixed flame. Int J Hydrogen Energy. 2013;38:5961–73.
19. Chen S, Liu ZH, Liu JZ, Li J, Wang L, Zheng CG. Analysis of entropy generation in hydrogen-enriched ultra-lean counter-flow methane–air non-premixed combustion. Int J Hydrogen Energy. 2010;35(22):12491–501.
20. Smith GP, Golden DM, Frenklach M, Moriarty NW, Eiteneer B, Goldenberg M, et al., GRI 3.0. http://www.me.berkeley.edu/gri_mech/.
21. CHEMKIN-PRO 15131 (2013) Reaction design: San Diego.
22. Zhang JC, Abraham J. A numerical study of laminar flames propagating in stratified mixtures. Combust Flame. 2016;163:461–71.
23. Liu FS, Ai YH, Kong WJ. Effect of hydrogen and helium addition to fuel on soot formation in an axisymmetric coflow laminar methane/air diffusion flame. Int J Hydrogen Energy. 2014;39(8):3936–46.
24. Doanh NAK, Swaminathan N. Autoignition and flame propagation in non-premixed MILD combustion. Combust Flame. 2019;201:234–43.
25. Cheng ZX, Wehrmeyer JA, Pitz RW. Experimental and numerical studies of opposed jet oxygen-enhanced methane diffusion flames. Combust Sci Technol. 2006;178(12):2145–63.
26. Padilla RE, Escofet-Martin D, Pham T, Pits WJ, Dunn-Rankin D. Structure and behavior of water-laden CH4/air counterflow diffusion flames. Combust Flame. 2018;196:439–51.
27. Hirschfelder JO, Cutiss CF, Byron RB. Molecular theory of gases and liquid. New York: Wiley; 1964.
28. Nishida K, Takagi T, Kinoshita S. Analysis entropy generation and exergy loss during combustion. Proc Combust Inst. 2002;29:869–74.
29. Bejan A, Kestin J. Entropy generation through heat and fluid flow. New York: Wiley; 1982.